



Communication

# Cyclic Plasticity of the As-Built EOS Maraging Steel: Preliminary Experimental and Computational Results

Barry Mooney <sup>1</sup>, Dylan Agius <sup>2</sup> and Kyriakos I. Kourousis <sup>1,\*</sup><sup>1</sup> School of Engineering, University of Limerick, V94 T9PX Limerick, Ireland; barrymooney.bm@gmail.com<sup>2</sup> Faculty of Engineering, University of Bristol, Bristol BS8 1TR, UK; dylan.agius@bristol.ac.uk

\* Correspondence: kyriakos.kourousis@ul.ie; Tel.: +353-61-202217

Received: 21 January 2020; Accepted: 4 February 2020; Published: 12 February 2020



**Abstract:** This short communication offers a preliminary view on ongoing research conducted on the as-built EOS maraging steel 300. The material's cyclic elastoplastic characteristics under strain-controlled loading have been investigated experimentally. Specimens fabricated under two primary orientations, horizontally and vertically to the build plate, have been tested. The obtained stress–strain hysteresis loops exhibited symmetry, with the vertical specimen showing a higher plastic strain energy dissipation capability than the horizontal specimen. Modelling of the material's elastoplastic behaviour was performed with a commonly used kinematic hardening rule, combined with both isotropic and anisotropic yield functions and elasticity moduli. The obtained simulations of the hysteresis loops, from the implementation of these two plasticity models, indicate the advantage of the anisotropic modelling approach over the isotropic approach. The anisotropic plasticity model describes in a more representative way the inherent elastic and plastic anisotropy of the as-built material. Further research is underway to explore the low cycle fatigue performance of this additively manufactured metal.

**Keywords:** maraging steel; plasticity; cyclic loading; low cycle fatigue; additive manufacturing

## 1. Introduction

Maraging steel 300 (MS300), also codified as American Iron and Steel Institute (AISI) 18Ni300, is an alloy typically used for structural components requiring very high strength, such as tooling, moulds, aircraft landing gear, and rocket casings. MS300 has been popular in laser powder bed fusion (LPBF) additive manufacturing (AM), mainly due to its good weldability. As with most AM alloys, there has been substantial research conducted on the characterisation of the MS300's mechanical properties under monotonic and cyclic loading. In the literature, a wide array of results can be found on its monotonic (tensile/compressive) performance, e.g., [1–6], while cyclic response results have mostly been reported for its high cycle fatigue (HCF) performance (in the range of  $10^5$ – $10^6$  cycles, with the imposed stress/strain remaining within the elastic regime), e.g., [4,7–9]. However, for the full characterisation of the material's mechanical properties, it is necessary to investigate its performance under cyclic loading.

Published work on the performance of MS300 under low cycle fatigue (LCF) conditions (material loaded up to  $10^3$  cycles within the elastoplastic regime) is currently limited to a single study [10]. In particular, the work of Branco et al. [10] identified the strain-controlled LCF characteristics of as-built MS300 produced with a Concept Laser M3 AM system. This study was limited to the examination of test coupons that were fabricated by having their loading axis vertically to the built plate (vertical orientation).

The present short communication reports a preliminary set of experimental and simulation results obtained from an ongoing cyclic plasticity/LCF testing campaign on as-built MS300 produced with

the EOS EOSINT M280 system. In particular, the experimental data from strain-controlled tests on vertically and horizontally fabricated test coupons are presented, analysed and discussed. This work offers an early look at experimental data examining the cyclic elastoplastic characteristics of this additively manufactured metal, complementing and extending the existing dataset of Branco et al. [10]. It also allows a comparison with a subset of the same previously published data and the evaluation of anisotropic plasticity modelling for simulation purposes. An isotropic plasticity modelling approach is commonly used by researchers and industry practitioners; however, it is a practice that may lead to higher computation error, which could, consequently, contribute to a substantial over- or under-estimation of the LCF life of this metal and parts produced with it.

## 2. Materials and Methods

The material used was MS1 (MS300) powder supplied by a metal AM equipment manufacturer (EOS). The powder consisted of spherical ( $36.69 \mu\text{m}$  median diameter) particles and had the chemical composition shown in Table 1 [5].

**Table 1.** Chemical composition of the MS1 (MS300) powder used.

	Ni	Mo	Co	Ti	Al	Cr	Mn	C	Fe
<b>MS1 (MS300)</b>	18.14	5.67	8.94	0.87	0.05–0.15	$\leq 0.5$	$\leq 0.01$	$\leq 0.03$	Balance

Rectangular test coupons (compliant with the ASTM E8M standard) were fabricated with EOS EOSINT M280 at the South Eastern Applied Materials (SEAM) Research Centre of the Waterford Institute of Technology. The geometry, dimensions and tolerances of the test coupons are illustrated in Figure 1. The EOS-recommended ‘MS1 Performance 2.0’ set of manufacturing parameters was used. The test coupons were fabricated at vertical and horizontal orientations relative to the build plate, with this communication reporting experimental data from a single set (one vertically and one horizontally produced test coupon). For simplicity, the test coupons are denoted as horizontal and vertical. Surface finishing was performed on the coupons via grinding and computer numerically controlled (CNC) wire electrical discharge machining (EDM) [5].

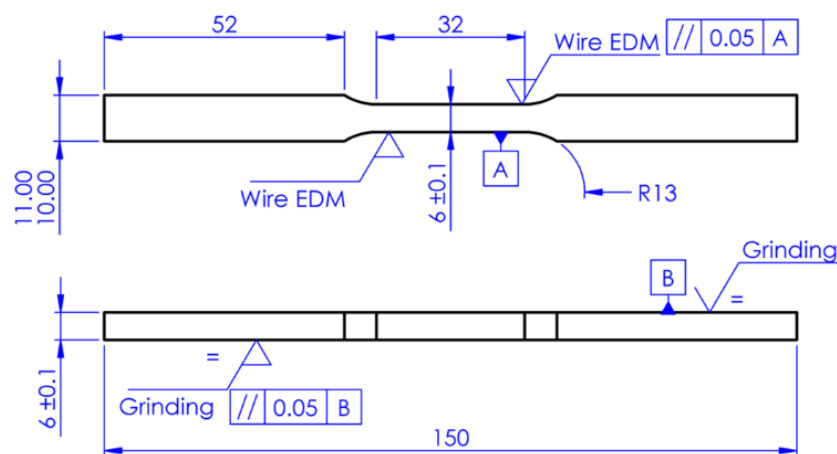


**Figure 1.** Test coupon geometry, dimensions and tolerances (in mm).

The mechanical tests were conducted at room temperature with a Zwick/Roell (Dartec) M1000/RK 100 kN servo-hydraulic closed-loop uniaxial testing machine fitted with  $\pm 100$  kN fatigue rated hydraulic wedge grips. The two test coupons were subjected to fully reversed ( $R = -1$ , where  $R$  is the ratio of maximum to minimum strain) strain-controlled cyclic loading within a  $\pm 0.9\%$  strain range for the horizontal and  $\pm 0.95\%$  for the vertical test coupon.

A microstructural analysis of the material of these specimens was not performed, as this has already been covered in our previously published studies for the same material [5,11].

### 3. Cyclic Plasticity Mathematical Modelling

The cyclic elastoplastic response of the material was mathematically modelled with a three term Armstrong–Frederick [12] kinematic hardening rule. The uniaxial formulation of this kinematic hardening rule is described by Equation (1), where  $X_i$  is the back-stress,  $c_i$  and  $\gamma_i$  are the material parameters and  $d\varepsilon^p$  is the incremental plastic strain:

$$dX_i = c_i d\varepsilon^p - \gamma_i X_i |d\varepsilon^p|, \text{ for } i = 1, 3 \tag{1}$$

Two types of yield surfaces ( $f$ ) have been used for a separate implementation and analysis, the isotropic von Mises, combined with isotropic elasticity (a single value for the Elasticity Modulus,  $E$ ), and the anisotropic Hill [13] (described by Equation (2)), combined with a Hooke’s law orthotropic Elasticity Modulus (described by Equation (3)). For brevity, the two models are referred to in the paper as the isotropic and the anisotropic plasticity model.

$$f = F(\sigma_{22} - \sigma_{33})^2 + G(\sigma_{33} - \sigma_{11})^2 + H(\sigma_{11} - \sigma_{22})^2 + 2(L\sigma_{23}^2 + M\sigma_{31}^2 + N\sigma_{12}^2) = 1/2 \tag{2}$$

where  $\sigma_{ij}$  are the stress components and  $F, G, H, L, M$  and  $N$  are the coefficients of the Hill anisotropic yield surface.

$$\begin{bmatrix} \varepsilon_{11} \\ \varepsilon_{22} \\ \varepsilon_{33} \\ 2\varepsilon_{23} \\ 2\varepsilon_{31} \\ 2\varepsilon_{12} \end{bmatrix} = \begin{bmatrix} \frac{1}{E_1} & -\frac{\nu_{21}}{E_2} & -\frac{\nu_{31}}{E_3} & 0 & 0 & 0 \\ -\frac{\nu_{12}}{E_1} & \frac{1}{E_2} & -\frac{\nu_{32}}{E_3} & 0 & 0 & 0 \\ -\frac{\nu_{13}}{E_1} & -\frac{\nu_{23}}{E_2} & \frac{1}{E_3} & 0 & 0 & 0 \\ 0 & 0 & 0 & \frac{1}{G_{23}} & 0 & 0 \\ 0 & 0 & 0 & 0 & \frac{1}{G_{13}} & 0 \\ 0 & 0 & 0 & 0 & 0 & \frac{1}{G_{12}} \end{bmatrix} \begin{bmatrix} \sigma_{11} \\ \sigma_{22} \\ \sigma_{33} \\ \sigma_{23} \\ \sigma_{31} \\ \sigma_{12} \end{bmatrix} \tag{3}$$

where  $\varepsilon_{ij}$  are the components of strain,  $E_i$  are the Elasticity Modulus’ tensor components in the direction of loading,  $\nu_{ij}$  are the Poisson ratios for extension in the  $i$  and  $j$  directions and  $G_{ij}$  are the Shear Modulus components in direction  $j$  on the plane whose normal is in direction  $i$ .

The anisotropic yield surface and orthotropic Hooke’s law (anisotropic model) were selected to allow the implementation of previously identified and measured plastic and elastic anisotropic parameters of the MS300 material [5]. The isotropic model was used as a benchmark to the anisotropic plasticity model in order to evaluate the latter model’s simulation accuracy.

## 4. Results and Discussion

### 4.1. Cyclic Mechanical Testing

The as-built EOS MS300 test coupons were strained to failure; however, only the data corresponding to the 28th cycle are reported and have been used in this analysis. This was a deliberate choice, since unplanned interruptions of the tests at the 29th cycle and the 516th cycle for the vertically and the horizontally built test coupons, respectively, may have compromised both the evolution of the hysteresis (stress–strain) loops and the LCF life of the material. Nevertheless, the 28th cycle data were sufficient to illustrate the cyclic elastoplastic characteristics of this material and to allow a comparison with the Branco et al. [10] mid-life (32nd cycle) results for the same strain range ( $\pm 0.9\%$ ) or close to that (i.e.,  $\pm 0.95\%$  for the vertical coupon). The obtained stress–strain hysteresis loops along with the aforementioned Branco et al. [10] experimental data are illustrated in Figure 2.

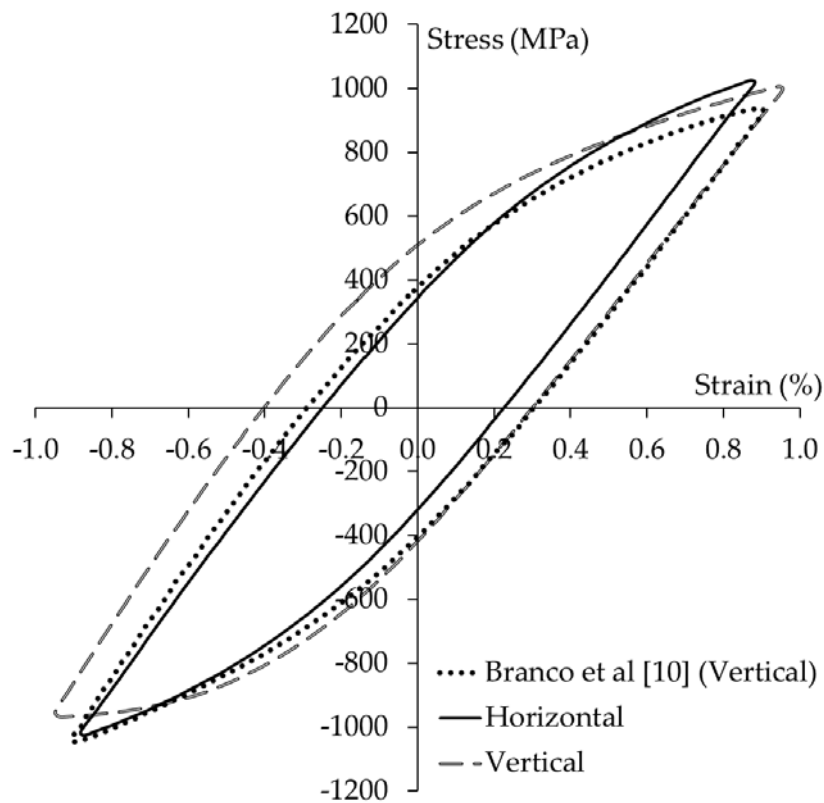


**Figure 2.** The hysteresis loops of the tested as-built EOS MS300 horizontal and vertical test coupons (at the 28th cycle) and the Branco et al. [10] published data for the as-built MS300 vertical coupon.

The hysteresis loops of the tested coupons (vertical, horizontal) appear to have symmetry, both in terms of their shape and in absolute stress values (approximately 900 and 1000 MPa, respectively). It can be observed that this is not the case for the Branco et al. [10] data, as the hysteresis loop has a negative stress asymmetry of approximately 100 MPa. Of note is that the area enclosed by the hysteresis loops, representing the plastic strain energy dissipation, is considerably smaller for the horizontal and the Branco et al. [10] vertical coupon compared to that of the vertical coupon. This is an indication of a higher LCF resistance of the vertical coupon; however, safe conclusions cannot be made unless further tests are performed for the estimation of the LCF life of as-built EOS MS300.

#### 4.2. Cyclic Plasticity Simulation

The parameters of the kinematic hardening rule (Equation (1)), used in both the isotropic and anisotropic plasticity model, were calibrated manually (employing a successive trial and error continuous optimisation approach) from the experimental hysteresis loop data (for the vertical coupon). These parameters are listed in Table 2. Moreover, the yield stress was calibrated to  $\sigma_y = 420$  MPa to account for the cyclic properties of the material (as opposed to using the yield stress measured from monotonic tensile tests).

**Table 2.** Parameters of the kinematic hardening rule for the as-built EOS MS300, used in both the isotropic and the anisotropic plasticity model.

Kinematic Hardening			
$c_1$	241,800 MPa	$\gamma_1$	930
$c_2$	98,280 MPa	$\gamma_2$	945
$c_3$	14,112 MPa	$\gamma_3$	96

For the isotropic hardening model, the Elasticity Modulus,  $E$ , selected was 160 GPa and the Poisson ratio,  $\nu$ , was 0.35 (based on the data reported in [5]).

The coefficients of the Hill anisotropic yield surface (Equation (2)) and the orthotropic Hooke's law (Equation (3)) (anisotropic plasticity model) were obtained from a previously published paper [11] on the same material (as-built EOS MS300). These coefficients are listed in Table 3. The methodology for the calculation of these coefficients is outside the scope of this paper; therefore, the reader is referred to the same publication for a detailed description [11].

**Table 3.** Coefficients of the Hill anisotropic yield surface and the orthotropic Hooke's law tensor for the as-built EOS MS300, used in the anisotropic plasticity model [12].

Hill		Orthotropic Hooke			
<b>F</b>	0.798	<b>E<sub>1</sub></b>	137 GPa	$\nu_{12}$	0.43
<b>G</b>	0.638	<b>E<sub>2</sub></b>	161 GPa	$\nu_{21}$	0.93
<b>H</b>	0.202	<b>E<sub>3</sub></b>	122 GPa	$\nu_{13}$	0.26
<b>L</b>	1.167	<b>G<sub>12</sub></b>	122 GPa	$\nu_{31}$	0.01
<b>M</b>	1.500	<b>G<sub>12</sub></b>	122 GPa	$\nu_{23}$	0.24
<b>N</b>	1.500	<b>G<sub>23</sub></b>	122 GPa	$\nu_{32}$	0.35

The two plasticity models were implemented for this study's experimental data (hysteresis loops stress–strain curves), derived from the two tested coupons (horizontal, vertical). Figure 3 presents the simulation results, where a good prediction of the experimental data can be observed. Of particular interest is that a closer prediction was obtained with the anisotropic plasticity model, which is attributed to the more representative description of the (elastic and plastic) anisotropy of the as-built EOS MS300 (measured in [5]). This is more clearly evidenced in the case of the horizontal test coupon data, where the hysteresis loop is simulated very well.

This, qualitative comparison is complemented by a calculation of the average error between experimental and simulated data (across the range of the stress–strain curve). The results of this calculation are included in Table 4, where the clear advantage of adopting the anisotropic plasticity model over the isotropic model is confirmed again.

**Table 4.** Average error (%) for the vertical and horizontal test coupon experimental and simulation data for the isotropic and the anisotropic plasticity model.

	Isotropic	Anisotropic
<b>Vertical</b>	43.5%	36.3%
<b>Horizontal</b>	58.6%	21.1%

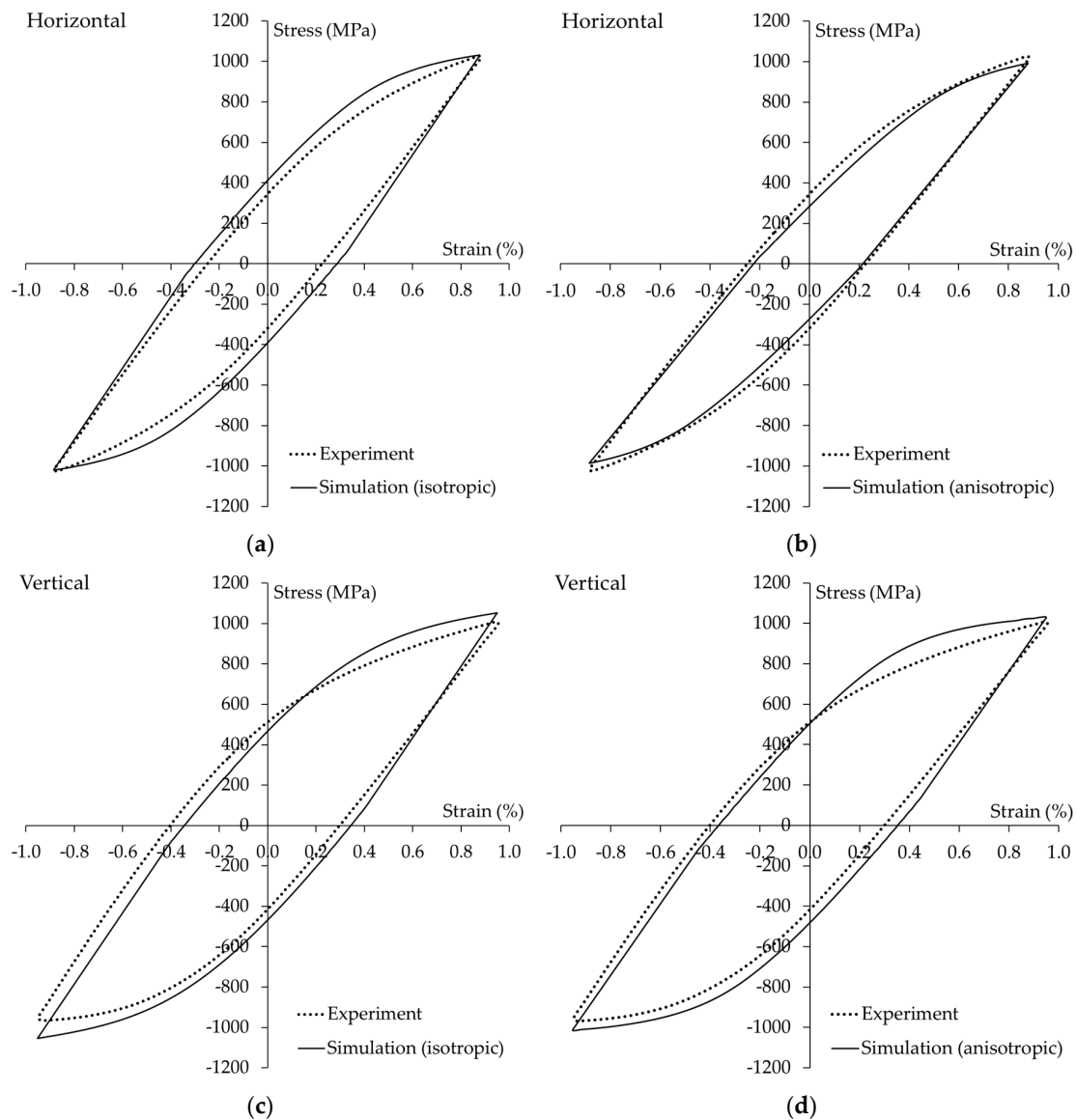


**Figure 3.** Experimental versus simulation results for the (a) isotropic plasticity model for the horizontal coupon; (b) anisotropic plasticity model for the horizontal coupon; (c) isotropic plasticity model for the vertical coupon; and (d) anisotropic plasticity model for the vertical coupon.

## 5. Conclusions

The obtained experimental and simulation results for the as-built EOS MS300 and the analysis have identified the following important features for this material:

- The stress–strain hysteresis loops produced from cyclic elastoplastic strain loading exhibited symmetrical characteristics, for both horizontal and vertical test coupons.
- Vertical test coupons appear to have a higher capacity for plastic strain energy dissipation than horizontal coupons, as indicated by their hysteresis loop area.
- The plasticity models used in this study were capable of simulating the hysteresis loops well.
- The anisotropic plasticity model offers a more representative description of the mechanical behaviour of this metal, resulting in higher accuracy simulations than the isotropic model.

A strain-controlled test campaign is ongoing, where coupons subjected to various strain ranges will be tested until failure. This will allow the estimation of the LCF life of the material, along with

obtaining stress–strain hysteresis loops. The results and findings from this experimental investigation are expected to be reported in a subsequent full research paper.

**Author Contributions:** Conceptualization, K.I.K.; methodology, B.M., D.A. and K.I.K.; software, D.A. and K.I.K.; validation, B.M., D.A. and K.I.K.; formal analysis, B.M., D.A. and K.I.K.; investigation, B.M., D.A. and K.I.K.; resources, B.M., D.A. and K.I.K.; data curation, B.M., D.A. and K.I.K.; writing—original draft preparation, B.M., D.A. and K.I.K.; writing—review and editing, B.M., D.A. and K.I.K.; visualization, B.M., D.A. and K.I.K.; supervision, K.I.K.; project administration, K.I.K.; funding acquisition, K.I.K. and B.M. All authors have read and agreed to the published version of the manuscript.

**Funding:** This research was partially funded by the Irish Research Council, through the Government of Ireland Postgraduate Research Programme, and the Faculty of Science and Engineering of the University of Limerick.

**Acknowledgments:** The support of the South Eastern Applied Materials (SEAM) Research Centre, of the Waterford Institute of Technology, in manufacturing the test coupons is acknowledged.

**Conflicts of Interest:** The authors declare no conflict of interest.

## References

1. Casati, R.; Lemke, J.N.; Tuissi, A.; Vedani, M. Aging behaviour and mechanical performance of 18-Ni 300 steel processed by selective laser melting. *Metals* **2016**, *6*, 218. [[CrossRef](#)]
2. Becker, T.H.; Dimitrov, D. The achievable mechanical properties of SLM produced Maraging Steel 300 components. *Rapid Prototyp. J.* **2016**, *22*, 487–494. [[CrossRef](#)]
3. Tan, C.; Zhou, K.; Ma, W.; Zhang, P.; Liu, M.; Kuang, T. Microstructural evolution, nanoprecipitation behavior and mechanical properties of selective laser melted high-performance grade 300 maraging steel. *Mater. Des.* **2017**, *134*, 23–34. [[CrossRef](#)]
4. Suryawanshi, J.; Prashanth, K.G.; Ramamurty, U. Tensile, fracture, and fatigue crack growth properties of a 3D printed maraging steel through selective laser melting. *J. Alloys Compd.* **2017**, *725*, 355–364. [[CrossRef](#)]
5. Mooney, B.; Kourousis, K.I.; Raghavendra, R. Plastic anisotropy of additively manufactured maraging steel: Influence of the build orientation and heat treatments. *Addit. Manuf.* **2019**, *25*, 19–31. [[CrossRef](#)]
6. Song, J.; Tang, Q.; Feng, Q.; Ma, S.; Setchi, R.; Liu, Y.; Han, Q.; Fan, X.; Zhang, M. Effect of heat treatment on microstructure and mechanical behaviours of 18Ni-300 maraging steel manufactured by selective laser melting. *Opt. Laser Technol.* **2019**, *120*, 105725. [[CrossRef](#)]
7. Croccolo, D.; De Agostinis, M.; Fini, S.; Olmi, G.; Robusto, F.; Kostic, S.C.; Vranic, A.; Bogojevic, N. Fatigue response of as-built DMLS maraging steel and effects of aging, machining, and peening treatments. *Metals* **2018**, *8*, 505. [[CrossRef](#)]
8. Damon, J.; Hanemann, T.; Dietrich, S.; Graf, G.; Lang, K.-H.; Schulze, V. Orientation dependent fatigue performance and mechanisms of selective laser melted maraging steel X3NiCoMoTi18-9-5. *Int. J. Fatigue* **2019**, *127*, 395–402. [[CrossRef](#)]
9. Croccolo, D.; De Agostinis, M.; Fini, S.; Olmi, G.; Robusto, F.; Ciric-Kostic, S.; Moraca, S.; Bogojevic, N. Sensitivity of direct metal laser sintering Maraging steel fatigue strength to build orientation and allowance for machining. *Fatigue Fract. Eng. Mater. Struct.* **2019**, *42*, 374–386. [[CrossRef](#)]
10. Branco, R.; Costa, J.D.M.; Berto, F.; Razavi, S.M.J.; Ferreira, J.A.M.; Capela, C.; Santos, L.; Antunes, F. Low-cycle fatigue behaviour of AISI 18Ni300 maraging steel produced by selective laser melting. *Metals* **2018**, *8*, 32. [[CrossRef](#)]
11. Mooney, B.; Kourousis, K.I.; Raghavendra, R.; Agius, D. Process phenomena influencing the tensile and anisotropic characteristics of additively manufactured maraging steel. *Mater. Sci. Eng. A* **2019**, *745*, 115–125. [[CrossRef](#)]
12. Armstrong, P.J.; Frederick, C.O. *A Mathematical Representation of the Multiaxial Bauschinger Effect*; G.E.G.B. Report RD/B/N 731; Berkeley, CA, USA, 1996.
13. Hill, R. A theory of the yielding and plastic flow of anisotropic metals. *Proc. R. Soc Lond. Ser. A Math. Phys. Sci.* **1948**, *193*, 281–297.

